The adsorption of ethyl formate on CaO: a DFT study

P. Bechthold[a,b], J. Juan[b,d], A. Juan[a,b,*], J. M. Marchetti[c]

[a] *IFISUR (UNS-CONICET), Av. Alem 1253, (8000) Bahía Blanca, Argentina*
[b] *Departamento de Física, Universidad Nacional del Sur, Av. Alem 1253, (8000) Bahía Blanca, Argentina*
[c] *Faculty of Science and Technology, Norwegian University of Life Sciences, Drøbakveien 31, 1432 Ås, Norway*
[d] *INFAP (CONICET), Av. Ejército de los Andes 950, (5700) San Luis , Argentina*

Abstract

Ethyl formate adsorption on CaO (001) is analyzed using Density Functional Theory (DFT) with Van der Waals corrections, implemented through the Vienna ab Initio Simulation Package (VASP). Our calculations reveals a possible adsorption site at low coverage with adsorption energy of $-1.21\,\mathrm{eV}$, which is more stable than ethanol and less stable than formic acid. Both molecular oxygens bond to two Ca atoms and the C methyl bonds to a surface oxygen. The analysis of the electronic structure and bonding show a stabilization of ethyl formate as a result of a shift in its states to lower energies, with respect to the gas phase. A relaxed molecular geometry is obtained after adsorption with no dissociation detected. There is a charge transfer (0.20 e) from the adsorbate to the surface. At the same time, H-C (formate) experiences a charge decrease of 0.16 e. The Ca-O in the surface mostly shows a decrease in bond order after adsorption.

Keywords: *CaO*, Catalyst, Ethyl formate, Adsorption, DFT

1. Introduction

Due to the need for reduction in greenhouse gas emissions, several new technological solutions are being considered as substitutes for petroleum-based fuels.

*Corresponding author
Email address: cajuan@uns.edu.ar (A. Juan)

In addition, international agreements have been made to reduce these emissions to zero by 2050 [1, 2].

Among all the different possibilities for new fuels, biodiesel is a key element as a substitute for diesel, with special interest for heavy-duty engines [3, 4]. Biodiesel is a renewable fuel that is produced from vegetable oils, animal fats, or recycled cooking oils in the presence of an alcohol and a catalysts [5–7]. Despite its promising environmental benefits, the current state of biodiesel production faces several challenges. One of the main concerns is competition with food crops for land and resources [8], which could potentially lead to food shortages and increased food prices. This concern is particularly relevant in developing countries, where food security is a major issue. Another challenge is ensuring the sustainability of biodiesel production, as the expansion of palm oil plantations for biodiesel has been associated with deforestation and habitat loss for endangered species [9]. Finally, biodiesel production can be heavily influenced by fluctuations in the price of petroleum diesel, which can make it difficult to predict profitability and investment returns [10].

Moreover, the use of certain feedstocks for biodiesel production, such as palm oil, contributes to deforestation and habitat loss for endangered species [9]. The high water and energy requirements of some biodiesel production processes are also a concern, as they potentially undermine the environmental benefits of biodiesel [10].

Catalysis is an essential component of biodiesel production, as it enables the transesterification of vegetable oils or animal fats with an alcohol to produce fatty acid alkyl esters (FAAEs). However, the use of certain catalysts can be associated with several problems that must be addressed to optimize the production process. One of the most widely used catalysts is sodium hydroxide (NaOH), which is effective and inexpensive [11]. However, NaOH requires careful handling, as it is a strong alkali that can cause severe burns and eye damage. In addition, the disposal of waste materials containing NaOH can pose environmental hazards [11]. Another commonly used catalyst is potassium hydroxide (KOH), which is also effective and can produce high yields of FAMEs

[11]. However, KOH is more expensive than NaOH, and its production can be energy-intensive. Other catalysts that have been investigated for biodiesel production include sulfuric acid, which can lead to corrosion and is hazardous to handle, and enzymes, which can be expensive and may require specific conditions to function effectively [11].

Due to the high demands of washing and purification from the homogeneous catalyst, heterogeneous catalysts are gaining more and more relevance, especially those that are being produced from renewable sources such as CaO. This catalyst is an alternative that has shown promise for use in biodiesel production. CaO is derived from a relatively abundant and inexpensive material (calcium carbonate) and can be easily regenerated and reused. Studies have shown that CaO can produce high yields of FAMEs from various feedstocks, including waste cooking oil, palm oil, and jatropha oil [12]. CaO has also been found to have several advantages over traditional catalysts such as sodium hydroxide and potassium hydroxide, including lower toxicity and reduced waste generation. Sanchez et al. [13] studied the transformation of jojoba oil using Calcium Oxide (CaO) derived from mussel shells, achieving a yield of 95%. Even though this yield is high, the reaction time was long as well (10 hours), and the alcohol used was methanol, which is typically produced from petroleum. To improve the process, Sanchez et al. [14] carried out the same reactions at a higher pressure. This permitted the yields to increase slightly to 96.3%, with a considerable reduction in the reaction time, from 10 to 5 hours.

Some work has been done on the analysis of DFT of biodiesel production [15], however, for this work the authors used an acid homogenous catalyst. Similarly, Li et al. [16] carried out calculations with DFT over heterogeneous catalysts; however, it was not to produce biodiesel but for the upgrading of bio-oils into second-generation biofuels. Similarly, Mao et al. [17] studied the migration of acyl groups when producing biodiesel; this was carried out to understand the migration of fatty acid chains within the triglyceride's molecule and not the production of biofuel itself. Other research works can also be found in the literature where DFT has been used to evaluate biodiesel reactions, such as

biodiesel oxidation/autoxidation [18, 19], and hydrogen-biodiesel interactions [20], among others.

To the best of our knowledge, glycerol-related interaction on CaO or rock salt basic solids is not well studied and therefore not fully understood [21, 22]. Orazi et al. [23] carried out a study using DFT modeling to analyze the interaction of the smallest fatty acid to understand the interactions of the acid functional group with the surface; this work has shown that the adsorption of the acid happens via the acid O-H bond, and this is the bond that breaks due to energy density. Similarly, Bechthold et al. [24] used DFT models to study the interaction of the ethyl group with the surface, showing that the adsorption could happen in two different locations, but in both cases, the O-H group of the alcohol is where the charge density will redistribute in such a way that this is the bond that will break. In this work, the ethyl formate molecule was studied using DFT over a CaO surface to understand its behavior and chemical interactions. The exposed surface studied was the (001) as previously reported [23, 24]. A study of the electronic charge and energy density, as well as bond length and strength, were carried out. Thus, understanding the adsorption behavior of ethylformate on the catalyst surface is essential for optimizing the reaction conditions and controlling the amount of solvent used in the reaction. By studying the adsorption kinetics and thermodynamics of ethylformate on the catalyst surface, researchers can gain insights into the mechanisms of the reaction and develop strategies to improve its efficiency and selectivity.

2. Computational Method

First-principles calculations based on spin-polarized DFT were performed using the Vienna Ab-initio Simulation Package (VASP) [25–27] to solve the Kohn-Sham equations with periodic boundary conditions. Core electrons were described by Blöchl projector augmented-wave (PAW) pseudopotentials [28, 29] while valence electrons were expanded from a plane-wave basis set with a kinetic energy cutoff of 800 eV. The exchange-correlation interactions were represented

through the Perdew–Burke–Ernzerhof functional with the generalized gradient approximation (GGA-PBE)[30]. Van der Waals interactions were accounted through DFT-D2 method by Grimme [31] with the following C_6, R_0 values for each element considered: H (0.14, 1.0001), C (1.75, 1.452), O (0.70, 1.342), Ca (10.80, 1.485) (in $Jnm^6\,mol^{-1}$ and Å respectively). The sampling of the Brillouin zone was done using the Monkhorst-Pack scheme [32] and a $(7 \times 7 \times 1)$ grid for all the calculations. Full geometry optimization was achieved relaxing ions through a conjugate gradient algorithm minimizing the system energy until it converged within 10^{-4} eV and the forces on each ion were less than $0.01\,\mathrm{eV/Å}$.

Ethyl formate adsorption at low coverage ($\approx 1/8$ ML) was simulated considering a 4×4 supercell with five layers, containing 80 Ca and 80 O atoms. The vacuum considered for avoid interaction with replicated cells, was set to 30 Å (see Figure S1 for a full view of the supercell utilized for all the calculations). A complete mapping over all the possible absorption sites of the CaO (001) surface was performed, considering in each case three different initial positions for the ethyl formate molecule (see Figures S2-S5 for all the tested configurations and energy values obtained at each site). In all cases the ethyl formate and the first four layers of the slab were relaxed. The selection of the CaO (001) surface as in previous works [23, 24], is because it is experimentally reported as the most stable.

The adsorption energy of the adsorbate over the CaO surface was calculated as follows:

$$E_{ads} = E(CaO + HCOOCH_2CH_3) - E(CaO) - E(HCOOCH_2CH_3) \quad (1)$$

where the first term on the right-hand side represents the energy of the supercell with the adsorbed $HCOOCH_2CH_3$ molecule. The second term is the total energy of the clean supercell (without the adsorbate) while the third term represents the energy of the ethyl formate molecule. To calculate the ethyl formate energy, we placed the molecule in a cubic box with 20 Å sides and performed a Γ-point calculation.

To understand the interactions between the ethyl formate and the CaO (001)

surface, we carried out a Density of States (DOS) analysis [33] to explore changes in energy levels during the adsorption process. Charges redistribution of the process was investigated through Bader analysis [34–36] while the change in bonds strength was analyzed by computing the Bond Order (BO) as implemented in the Density Derived Electrostatic and Chemical (DDEC6) method [37–40]

3. Results and discussion

3.1. CaO bulk and CaO (001)

In a recent study [23], we investigate the bulk properties of CaO through an analysis of its bulk lattice constants and electronic structure. Our results demonstrate a high degree of agreement between experimental data and computed values of these properties. Specifically, our calculations yield a lattice parameter of 4.84 Å for CaO in the NaCl-type (B1) structure with a space group of Fm-3 m, which is consistent with both theoretical works [21, 41, 42] and experimental data reported [43, 44] in the literature.

In addition to analyzing the bulk lattice constants, we also investigate the bonding scheme of the CaO (001) surface. Our results demonstrate again consistency with previous experimental works reported in the literature, further validating the accuracy of our computational approach.

3.2. Ethyl formate adsorption on CaO (001)

In this study, we examined the process of adsorption of ethyl formate on the previously optimized CaO (001) surface [23]. To explore this process, we conducted a comprehensive mapping of the possible adsorption sites on the surface. For each site, we considered three different possibilities of approach between the adsorbate (ethyl formate) and the surface, and we analyzed the resulting configurations in detail (refer to the supplementary material for additional information of all the sites and configurations tested for this surface).

Our computational analysis of the adsorption process revealed a preferential adsorption site for ethyl formate on the CaO (001) surface. Importantly, we

found that ethyl formate adsorbs on the surface without encountering an energy barrier during the relaxation process, starting from $C_3H_6O_2$ in the gas phase. Figure 1 provides a detailed representation of the adsorption site.

The computed adsorption energy for the minimum energy site found was $-1.21\,\text{eV}$. This configuration was by far more energetically stable than those obtained for the other tested sites, so the rest of the analysis will be carried out on this configuration.

As a first step, we investigate the structural effect of the ethyl formate adsorption on the CaO(001) surface. To that end, we analyze the bond lengths of the atoms involved in the process, before and after the ethyl formate adsorption. The respective bond distances and bond distance percentage change are summarized in Table 1. As can be seen in Figure 1, the adsorption of ethyl formate occurs mainly through the interaction of the adsorbate with the Ca33, O35, Ca58, and Ca53 atoms of the CaO(001) surface. Regarding the adsorbate, the bond distances that were most affected in the adsorption process were the ones relative to the C3 atom, with an increase of 14.07% for the C3-O81 bond and 6.56% for the C3-O82 bond. For the surface atoms, the bonds of the Ca atoms that bond with the adsorbate and its first neighbors were found to be the most affected. However, in no case was detected a variation greater than 10% in bond length compared with the pristine surface.

In addition to analyzing changes in bond distances, the degree of participation of each atom in the adsorption process was determined through a Bond Order (BO) analysis, which provides information about the strength of each bond. The most relevant BO and percentage change in BO obtained for the surface atoms and the adsorbate are summarized in Table 2.

Regarding the bonds of the adsorbate, it can be seen that the bond order between C1 and O81 shows an increase of 8.33% compared to its initial value, suggesting a tendency for the C1-O81 bond to become stronger. Additionally, the bond orders between C3 and O81, and between C3 and O82 decrease by 42.97% and 22.96% respectively, indicating a weakening of these bonds. This results indicate that the carbonyl group of ethyl formate is strongly interacting

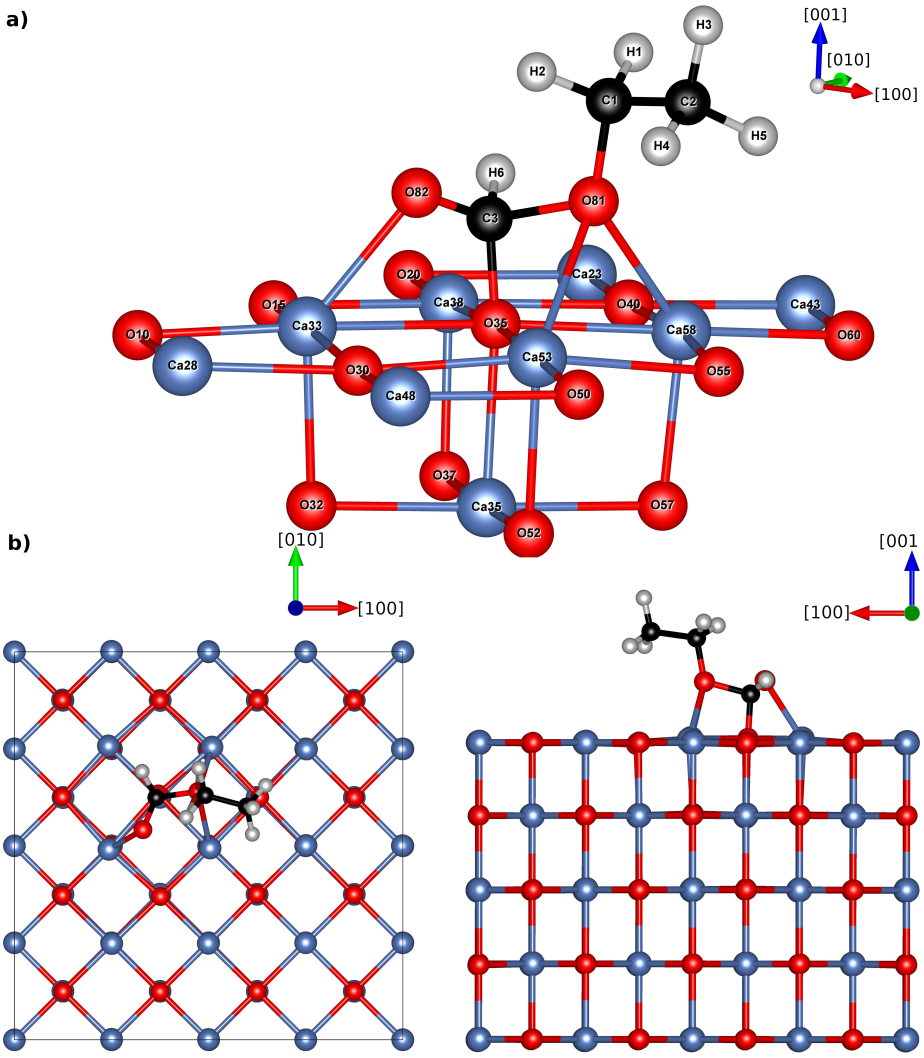

Figure 1: Different views of the ethyl formate adsorption site found on CaO (001): (a) magnification with atom labels, (b) top view, and (c) lateral view. Blue, red, black, and grey spheres represent Ca, O, C, and H atoms, respectively.

Table 1: Distances of the bonds of the CaO (001) surface and ethyl formate, before and after adsorption, along with the relative percentage change of the bonds (%Δ) during the process. The labels of the atoms are shown in Figure 1.

Group	Bond atoms		Distances (Å)		
			After	Before	%Δ
Ethyl formate	C1	H1	1.11	1.10	0.91
	C1	H2	1.10	1.10	0.00
	C1	C2	1.52	1.51	0.66
	C1	O81	1.43	1.46	-2.05
	C2	H3	1.10	1.10	0.00
	C2	H4	1.10	1.10	0.00
	C2	H5	1.10	1.10	0.00
	C3	H6	1.14	1.11	2.70
	C3	O81	1.54	1.35	14.07
	C3	O82	1.30	1.22	6.56
Bonds with surface	C3	O35	1.43	-	-
	O81	Ca53	2.74	-	-
	O81	Ca58	2.49	-	-
	O82	Ca33	2.33	-	-
Surface	Ca33	O10	2.31	2.42	-4.55
	Ca33	O15	2.49	2.42	2.89
	Ca33	O30	2.47	2.42	2.07
	Ca33	O35	2.62	2.42	8.26
	O35	Ca38	2.45	2.42	1.24
	O35	Ca53	2.64	2.42	9.09
	O35	Ca58	2.51	2.42	3.72
	Ca58	O40	2.48	2.42	2.48
	Ca58	O55	2.45	2.42	1.24
	Ca58	O60	2.31	2.42	-4.55
	Ca53	O30	2.45	2.42	1.24
	Ca53	O50	2.32	2.42	-4.13
	Ca53	O55	2.51	2.42	3.72

Table 2: Bond order (BO) values obtanied for the bonds of the CaO (001) surface and ethyl formate, before and after adsorption, along with the percentage change of BO (%Δ) of each bond during the process. The labels of the atoms are shown in Figure 1.

Group	Bond atoms		Bond order		
			After	Before	%Δ
Ethyl formate	C1	H1	0.85	0.84	1.19
	C1	H2	0.82	0.84	-2.38
	C1	C2	1.05	1.08	-2.78
	C1	O81	1.04	0.96	8.33
	C2	H3	0.93	0.92	1.09
	C2	H4	0.91	0.92	-1.09
	C2	H5	0.92	0.92	0.00
	C3	H6	0.76	0.86	-11.63
	C3	O81	0.73	1.28	-42.97
	C3	O82	1.51	1.96	-22.96
Bonds with surface	C3	O35	1.09	-	-
	O81	Ca53	0.07	-	-
	O81	Ca58	0.16	-	-
	O82	Ca33	0.25	-	-
Surface	Ca33	O10	0.33	0.27	22.22
	Ca33	O15	0.23	0.28	-17.86
	Ca33	O30	0.23	0.28	-17.86
	Ca33	O35	0.12	0.27	-55.56
	O35	Ca38	0.19	0.28	-32.14
	O35	Ca53	0.13	0.28	-53.57
	O35	Ca58	0.17	0.28	-39.29
	Ca58	O40	0.24	0.28	-14.29
	Ca58	O55	0.24	0.28	-14.29
	Ca58	O60	0.33	0.27	22.22
	Ca53	O30	0.25	0.27	-7.41
	Ca53	O50	0.33	0.28	17.86
	Ca53	O55	0.21	0.27	-22.22

with the CaO (001) surface, which may promote its dissociation.

As mentioned above, the binding with the CaO (001) surface is mainly achieved through the development of bonds with the O35, Ca53, Ca58, and Ca33 atoms on the surface, with the bond with the oxygen being the strongest. Additionally, the O35 atom, experiences a decrease in the BO with all the neighboring atoms of the surface, along with an elevation of 0.16 Å. The C3-O35 distance is 1.43 Å, which lies in between C-$O_{molecular}$ distance before adsorption. Also the O81-Ca58 (O82-Ca33) bond distances between molecule and surface are similar to those in the CaO clean surface (2.49-2.33 Å vs 2.42 Å). The bond angles around C3 change from an sp2 hybridization before adsorption to a distorted tetrahedral being C3-O81-O35: 100.62 °, C3-O82-O85: 115.3 ° and C3-O81-O82: 112.21 °.

Except the O35 atom, the remaining atoms on the surface involved in the bond with ethyl formate do not exhibit a uniform behavior in terms of the magnitude of the bonds. Specifically, the BO values between these atoms and their first neighbors increase in some cases and decrease in others. This behavior in the BO agrees with what was observed in the analysis of the bond lengths for the surface atoms and indicates that the most affected surface atom in the adsorption process turns out to be O35 with a clear tendency to form a bond with the adsorbate at the cost of a significant decrease in the amount of binding with the surface.

3.3. Electronic structure analysis

The electronic structure was analyzed to obtain more information about the bonds formed between ethyl formate and the surface during the adsorption process.

The total DOS of ethyl formate in the gas phase (before adsorption) is shown in Figure 2 (a). The electronic structure of the adsorbate consists of well-defined sharp peaks which extend into the range of -22 to 0 eV. The Figure 2 (b) displays the total density of states for the CaO (001) surface before adsorption, while in Figure 2 (c), the total DOS of the system after adsorption is shown. By

comparing the figures, it can be seen that there is a hybridization of states near the Fermi level and the -20 eV zone. These peaks are composed of s-type and p-type states, as can be seen in the projected DOS (PDOS) for the adsorbate in Figure 3 (a) and (e), respectively. After adsorption (Figure 3 (b) and (f)), hybridization of s and p states is observed in both the vicinity of the Fermi level and the -20 eV range. Furthermore, a slight shift towards lower energies is detected for the s states, which is an indicator of the stabilization of said states of the adsorbate.

The hybridization involves both the p and s states of the surface, as can be seen by comparing Figure 3 (c-d) and (g-h). This indicates that both the s and p states of the surfaces are involved in the binding with the adsorbate. The d-states of the surface did not undergo significant modifications during adsorption; as a result, they were not reported. It is important to note that neither the surface nor the adsorbate exhibited an appreciable magnetic moment. This is why, in all cases, only one spin orientation was plotted for the density of states. The overall effect of the adsorption of ethylformate on the CaO electronic configuration can be appreciated in more detail in Figure 4, where the density of states is projected only onto the atoms involved in the adsorption process. Comparing Figure 4 (a) and (b), we can appreciate how the formate states become stabilized after adsorption (see peaks at -22 eV and near the Fermi level). Figure 4 (c) and (d) present the changes in Ca and O atoms from CaO (001) furface. There are several new peaks as a consequence of the adsorption and a broadering of the Ca p states at -20 eV.

The Bader charge analysis for the atoms involved in the bonding of ethyl formate with the CaO (001) surface is summarized in Table 3. The results revealed a general behavior, the charge of the surface atoms experienced a slight increase, while the adsorbate atoms exhibited a slight decrease in charge (indicating a transfer of electrons from the surface to the adsorbate). The net charge decrease in ethyl formate after adsorption is primarily attributed to variations in the charges of the H6 and O82 atoms, with values of -0.16 e and -0.13 e, respectively. In the case of the surface, the charge variation is mainly concen-

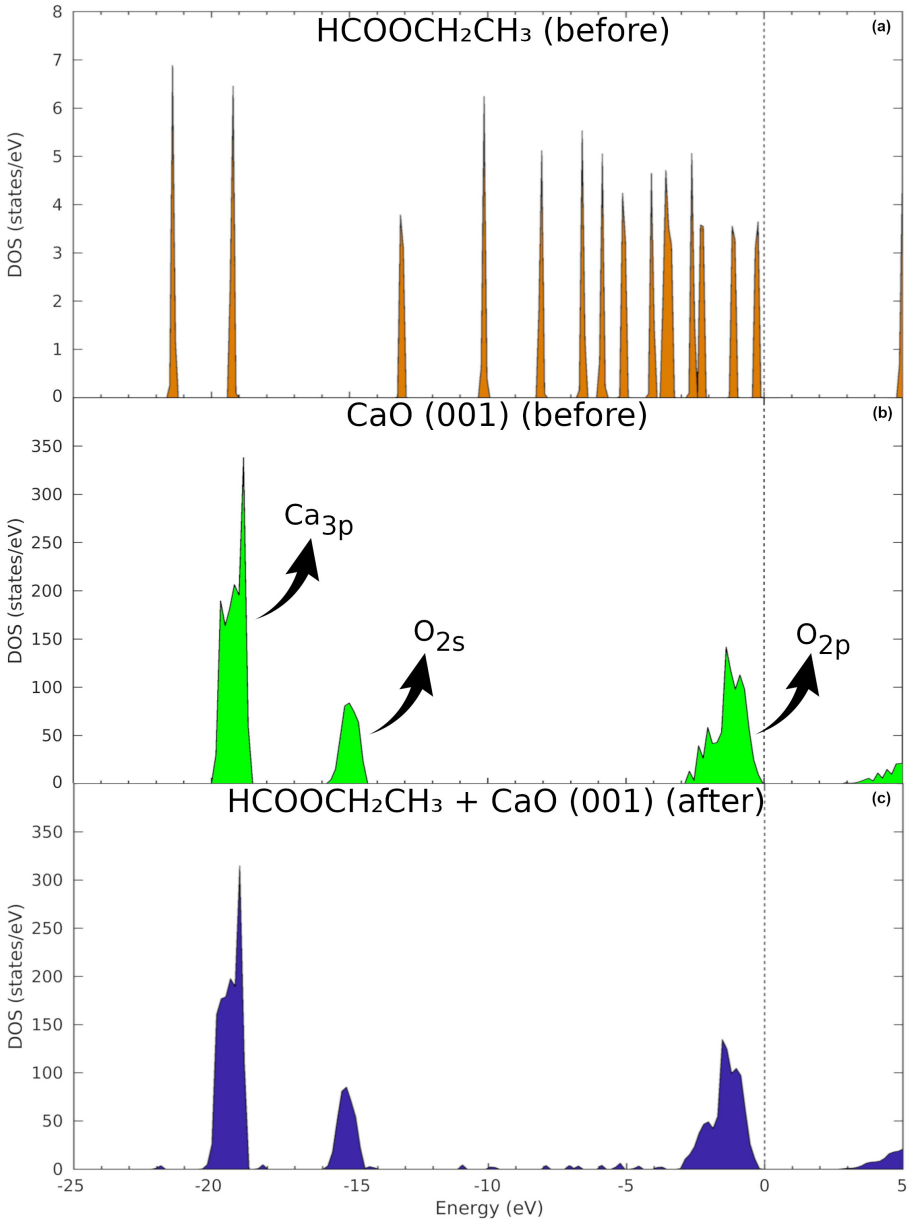

Figure 2: Total DOS for (a) $C_3H_6O_2$ in the gas phase, (b) CaO (001) before adsorption, and (c) the surface with the adsorbed ethyl formate. The dashed line indicates the Fermi level.

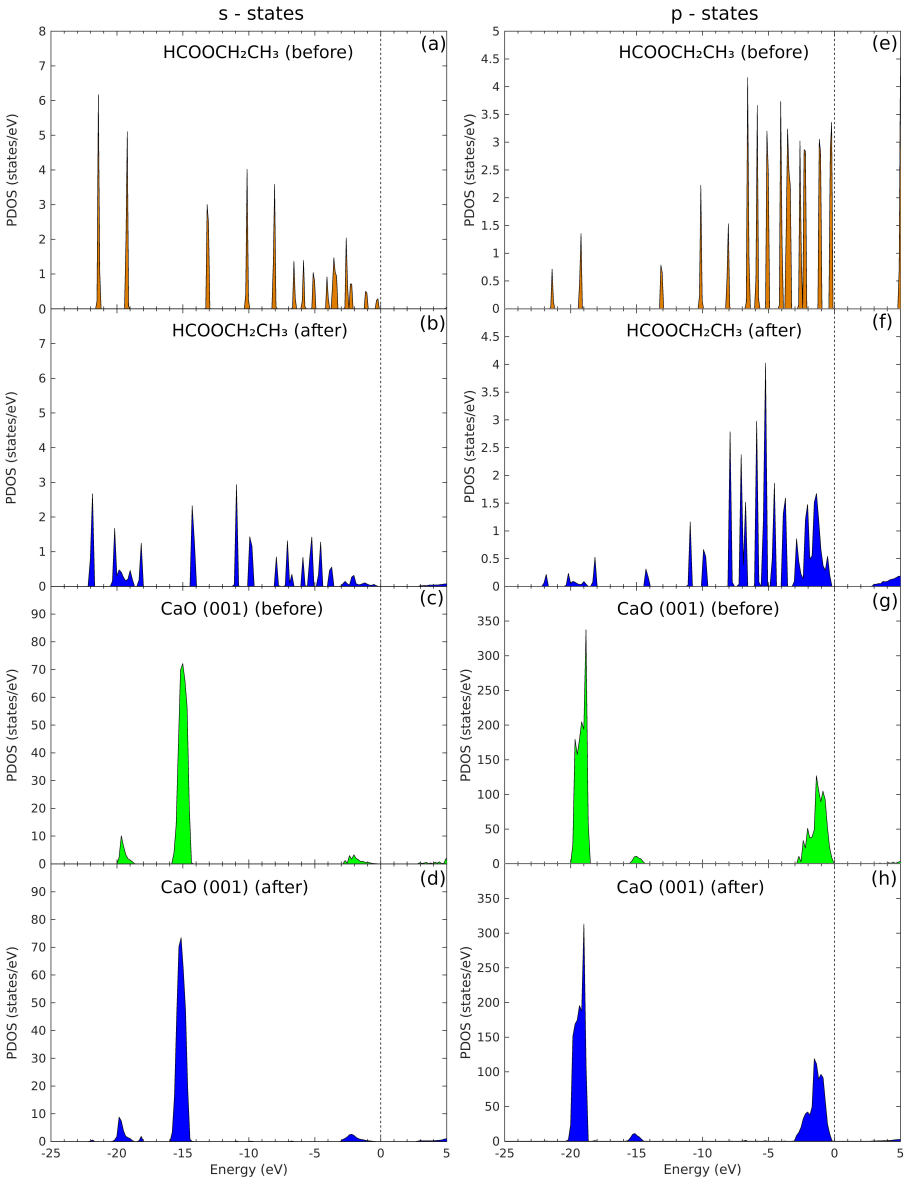

Figure 3: Projected DOS for CaO (001) and $C_3H_6O_2$, before and after adsorption, are shown in (a)-(d) for s-states projections, and in (e)-(h) for p-states projections. The dashed line indicates the Fermi level.

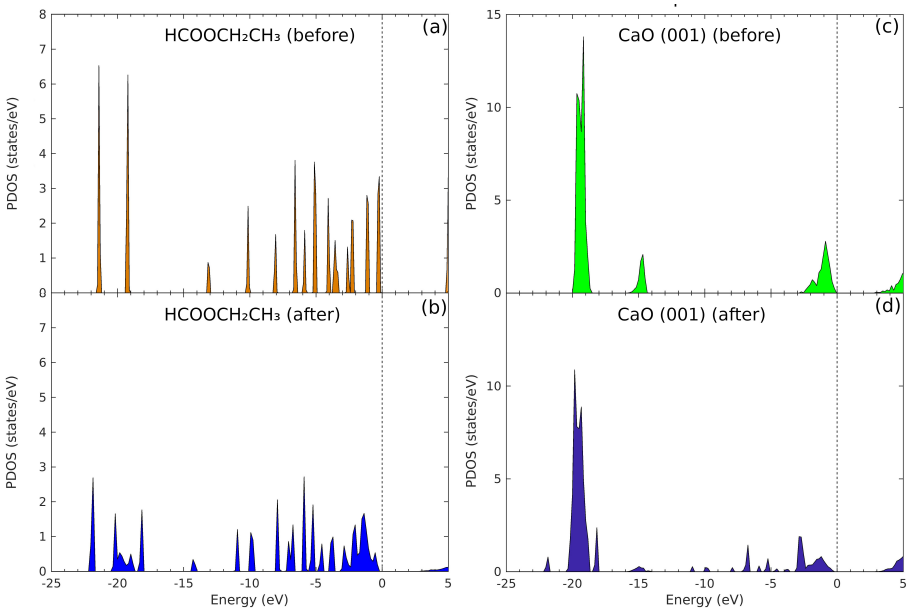

Figure 4: Projected DOS for ethyl formate atoms O81, O82 and C3 before (a) and after (b) adsorption. Projected DOS for CaO (001) atoms Ca33, Ca53, Ca55 and O35 before (c) and after (d) adsorption. The labels of the atoms are shown in Figure 1.

Table 3: Total Bader charge before and after adsorption. $\Delta(e)$ = (after - before), (+) win e, (−) lost e. The labels of the atoms are shown in Figure 1.

Group	Atom	After (e)	Before (e)	$\Delta(e)$
Ethyl formate	H1	0.02	0.06	-0.04
	H2	0.07	0.07	0.00
	H3	0.05	0.05	0.00
	H4	0.01	0.04	-0.03
	H5	0.02	0.03	-0.01
	H6	-0.05	0.11	-0.16
	C1	0.42	0.37	0.05
	C2	-0.07	-0.04	-0.03
	C3	1.48	1.50	-0.02
	O81	-1.04	-1.05	0.01
	O82	-1.27	-1.14	-0.13
Surface	Ca33	1.51	1.48	0.03
	Ca38	1.48	1.48	0.00
	Ca53	1.51	1.48	0.03
	Ca58	1.50	1.48	0.02
	O30	-1.46	-1.48	0.02
	O35	-1.28	-1.48	0.20
	O50	-1.48	-1.48	0.00
	O55	-1.45	-1.48	0.03
	O60	-1.48	-1.48	0.00

trated in the O35 atoms, with a value of +0.20 e, while the variation observed in other atoms involved in the adsorption did not exceed +0.03 e.

Beyond the general behavior of net charge transfer from the adsorbate to the surface (electrons from the surface to the adsorbate), these results suggest electronic redistribution due to the interaction between ethyl formate and the CaO (001) surface, indicating the influence of the adsorption process on the charge distributions.

Figure 5 presents the electron density charge difference of ethyl formate on CaO (001). This difference $\Delta\rho$ is calculated using the equation

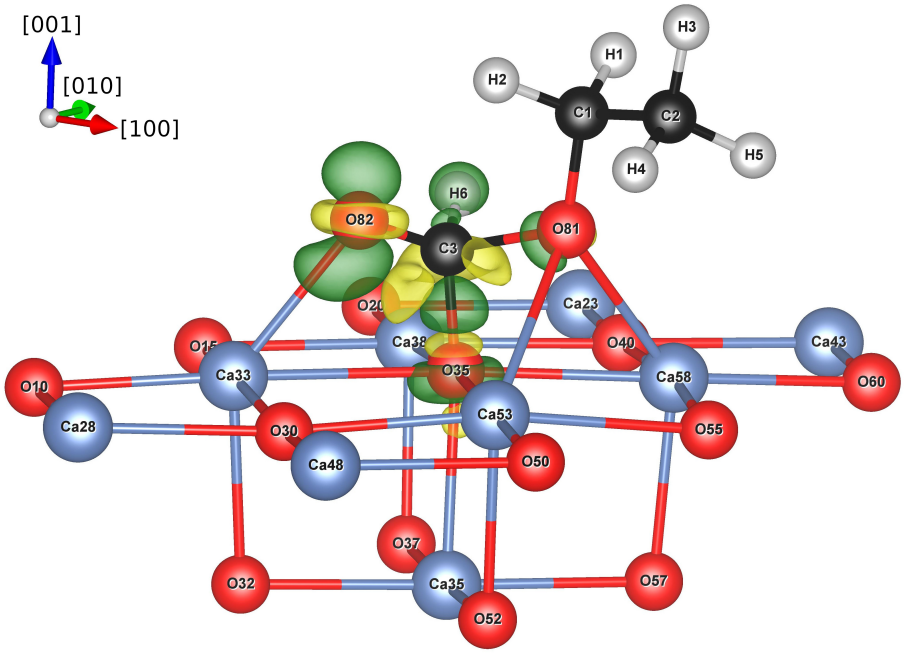

Figure 5: Electron charge density difference plot of ethyl formate adsorbed on CaO (001). The green color indicates positive charge while yellow indicates negative charge.

$$\Delta\rho = \rho(CaO + HCOOCH_2CH_3) - \rho(CaO) - \rho(HCOOCH_2CH_3) \quad (2)$$

where $\rho(CaO+HCOOCH_2CH_3)$ represents the charge density of the entire system in its most stable configuration, $\rho(HCOOCH_2CH_3)$ represents the charge density of isolated ethyl formate and $\rho(CaO)$ represents the charge density of the CaO (001) surface. This results are consistent with the Bader analysis, the isosurfaces shown in Figure 5 highlight the major changes in the charge of the atoms involved in the adsorption process. The green color indicates a loss of charge, while yellow indicates a gain in charge density. It can be noted that the main changes occurs around atoms O81, O82, C3, H6 (from the formate molecule) and O35 (from the surface).

4. Conclusions

The adsorption of ethyl formate on CaO (001) is a favourable process with an energy of $-1.21\,\mathrm{eV}$ that is higher (lower) than ethanol (formic acid) adsorption $-1.14\,\mathrm{eV}(-2.38\,\mathrm{eV})$. Among all tested sites and molecular configurations, we found that the bond with the surface involves two molecular oxygens and three Ca cations from the surface, and the C formate bonded to a surface oxygen. The C3-$O_{surface}$ distance is 1.43 Å, which is something in between C=O and C-O from the molecule (1.54 Å and 1.30Å respectively) which are elongated after adsorption. There is a charge transfer ($0.20\,e$) from the adsorbate to the surface. At the same time, H-C (formate) experiences a decrease of 0.16 e being the one with the greatest charge variation during the adsorption process. C3 changes its hybridization from sp^2 in the isolated molecule to a distorted tetrahedral bonded to three oxygens and one hydrogen. The molecule-surface bond is achieved by an important decrease in Ca-O surface bonds order.

Therefore, the results in this work indicate and explain the favorable adsorption of ethyl formate over the CaO surface, which in the future can be further studied regarding thermodynamics and kinetics based models in order to gain a deeper understanding of the optimization of this reaction for a better performance of application.

Author contributions

The manuscript was written through contributions of all authors. All authors have given approval to the final version of the manuscript.

Conflicts of interest

There are no conflicts to declare.

Acknowledgement

The simulations were performed on resources provided by UNINETT Sigma2 the National Infrastructure for High Performance Computing and Data Storage

in Norway. Our work was supported by ANPCyT through PICT 2019-03491, PICT 2021-I-A01144 and founded through the project UNPRECENDENTED HORIZON-MSCA-2021-SE-01-01 project number 101086363. PB, JJ and AJ are members of CONICET, J.M.M acknowledge NMBU Norway.

References

[1] European green deal, https://climate.ec.europa.eu/eu-action/european-green-deal_en.

[2] 2030 climate and energy framework, https://climate.ec.europa.eu/eu-action/climate-strategies-targets/2030-climate-energy-framework_en.

[3] B. Changmai, C. Vanlalveni, A. P. Ingle, R. Bhagat, S. L. Rokhum, Widely used catalysts in biodiesel production: a review, RSC advances 10 (68) (2020) 41625–41679.

[4] M. Ramos, A. P. S. Dias, J. F. Puna, J. Gomes, J. C. Bordado, Biodiesel production processes and sustainable raw materials, Energies 12 (23) (2019) 4408.

[5] A. Gholami, F. Pourfayaz, A. Maleki, Recent advances of biodiesel production using ionic liquids supported on nanoporous materials as catalysts: a review, Frontiers in Energy Research 8 (2020) 144.

[6] F. Moazeni, Y.-C. Chen, G. Zhang, Enzymatic transesterification for biodiesel production from used cooking oil, a review, Journal of cleaner production 216 (2019) 117–128.

[7] O. Aboelazayem, M. Gadalla, B. Saha, Biodiesel production from waste cooking oil via supercritical methanol: Optimisation and reactor simulation, Renewable Energy 124 (2018) 144–154.

[8] M. Balat, H. Balat, Progress in biodiesel processing, Applied Energy 87 (6) (2010) 1815–1835.

[9] L. Koh, J. Ghazoul, Biofuels, biodiversity, and people: Understanding the conflicts and finding opportunities, Biological Conservation 141 (2008) 2450–2460.

[10] P. S. Nigam, A. Singh, Production of liquid biofuels from renewable resources, Progress in Energy and Combustion Science 37 (1) (2011) 52–68.

[11] L. Meher, D. Vidya Sagar, S. Naik, Technical aspects of biodiesel production by transesterification—a review, Renewable and Sustainable Energy Reviews 10 (3) (2006) 248–268.

[12] W.-Y. Wong, S. Lim, Y.-L. Pang, S.-H. Shuit, M.-K. Lam, I.-S. Tan, W.-H. Chen, A comprehensive review of the production methods and effect of parameters for glycerol-free biodiesel production, Renewable and Sustainable Energy Reviews 182 (2023) 113397.

[13] M. Sánchez, J. M. Marchetti, M. Martínez, J. Aracil, Technoeconomic analysis of jatropha curcas integral valorization, Biofuels, Bioproducts and Biorefining 12 (4) (2018) 577–585.

[14] M. Sánchez, M. R. Avhad, J. M. Marchetti, M. Martínez, J. Aracil, Jojoba oil: A state of the art review and future prospects, Energy Conversion and Management 129 (2016) 293–304.

[15] T. Li, X. Zhang, C. Zhang, R. Li, J. Liu, H. Zhang, P. Han, Z. Zheng, C. Fan, A density functional theory study on the acid-catalyzed transesterification mechanism for biodiesel production from waste cooking oils, Journal of the American Oil Chemists' Society 96 (2) 137–145.

[16] X. Li, X. Luo, Y. Jin, J. Li, H. Zhang, A. Zhang, J. Xie, Heterogeneous sulfur-free hydrodeoxygenation catalysts for selectively upgrading the renewable bio-oils to second generation biofuels, Renewable and Sustainable Energy Reviews 82 (2018) 3762–3797.

[17] J. Mao, Z. Hu, J. Hu, X. Zhu, H. Xiong, A density functional theory (dft) study of the acyl migration occurring during lipase-catalyzed transesterifications, International Journal of Molecular Sciences 20 (14).

[18] V. M. L. dos Santos, J. A. B. da Silva, L. Stragevitch, R. L. Longo, Thermochemistry of biodiesel oxidation reactions: A dft study, Fuel 90 (2) (2011) 811–817.

[19] A. dos Reis Albuquerque, J. Maul, A. F. F. Vasconcelos, J. R. C. Filho, I. M. G. dos Santos, A. G. de Souza, The first step of biodiesel autoxidation by differential scanning calorimetry and dft calculations, Journal of Thermal Analysis and Calorimetry 117 (2) (2014) 799–806.

[20] L. Zhang, Q. Meng, Y. Chi, P. Zhang, Toward high-level theoretical studies of large biodiesel molecules: An oniom [qcisd (t)/cbs: Dft] study of the reactions between unsaturated methyl esters (c n h2 n–1cooch3) and hydrogen radical, The Journal of Physical Chemistry A 122 (21) (2018) 4882–4893.

[21] M. Calatayud, Ethylene glycol interaction on alkaline earth oxides: A periodic dft study, Catalysis Today 152 (1) (2010) 88–92, catalysis by Acids and Bases: new materials and surface studies ABC-6, 6th World Congress on Catalysis by Acids and Bases, Genova (Italy) May 10-14, 2009.

[22] M. Calatayud, A. Ruppert, B. Weckhuysen, Theoretical study on the role of surface basicity and lewis acidity on the etherification of glycerol over alkaline earth metal oxides, Chemistry – A European Journal 15 (41) (2009) 10864–10870.

[23] V. Orazi, A. Juan, E. A. Gonzalez, J. M. Marchetti, P. V. Jasen, Dft study of ethanol adsorption on cao (0 0 1) surface, Applied Surface Science 500 (2020) 144254.

[24] P. Bechthold, V. Orazi, A. Juan, J. Marchetti, A first-principles study of

formic acid adsorption on cao (001), Applied Surface Science 583 (2022) 152296.

[25] G. Kresse, J. Furthmüller, Efficient iterative schemes for ab initio total-energy calculations using a plane-wave basis set, Phys. Rev. B 54 (16) (1996) 11169–11186.

[26] G. Kresse, J. Hafner, Ab initio molecular dynamics for liquid metals, Phys. Rev. B 47 (1) (1993) 558–561.

[27] G. Kresse, J. Furthmüller, Efficiency of ab-initio total energy calculations for metals and semiconductors using a plane-wave basis set, Comput. Mater. Sci. 6 (1) (1996) 15–50.

[28] G. Kresse, D. Joubert, From ultrasoft pseudopotentials to the projector augmented-wave method, Phys. Rev. B 59 (1999) 1758–1775.

[29] P. E. Blöchl, Projector augmented-wave method, Phys. Rev. B 50 (1994) 17953–17979.

[30] J. Perdew, K. Burke, M. Ernzerhof, Generalized Gradient Approximation Made Simple., Phys. Rev. Lett. 77 (18) (1996) 3865–3868.

[31] S. Grimme, Semiempirical GGA-type density functional constructed with a long-range dispersion correction, J. Comput. Chem. 27 (15) (2006) 1787–1799.

[32] H. J. Monkhorst, J. D. Pack, Special points for Brillouin-zone integrations, Phys. Rev. B 13 (12) (1976) 5188–5192.

[33] R. Hoffman, Solids and Surfaces: A Chemist's View of Bonding in Extended Structures, Wiley-VCH, 1988.

[34] R. F. W. Bader, Atoms in Molecules, John Wiley & Sons, Ltd, Chichester, UK, 2002.

[35] G. Henkelman, A. Arnaldsson, H. Jónsson, A fast and robust algorithm for Bader decomposition of charge density, Comput. Mater. Sci. 36 (3) (2006) 354–360.

[36] M. Yu, D. R. Trinkle, Accurate and efficient algorithm for Bader charge integration, J. Chem. Phys 134 (6) (2011) 064111.

[37] T. A. Manz, N. G. Limas, Introducing DDEC6 atomic population analysis: part 1. Charge partitioning theory and methodology, RSC Adv. 6 (53) (2016) 47771–47801.

[38] N. G. Limas, T. A. Manz, Introducing DDEC6 atomic population analysis: part 2. Computed results for a wide range of periodic and nonperiodic materials, RSC Adv. 6 (51) (2016) 45727–45747.

[39] T. A. Manz, Introducing DDEC6 atomic population analysis: part 3. Comprehensive method to compute bond orders, RSC Adv. 7 (72) (2017) 45552–45581.

[40] N. G. Limas, T. A. Manz, Introducing DDEC6 atomic population analysis: part 4. Efficient parallel computation of net atomic charges, atomic spin moments, bond orders, and more, RSC Adv. 8 (5) (2018) 2678–2707.

[41] N. V. Skorodumova, K. Hermansson, B. Johansson, Structural and electronic properties of the (100) surface and bulk of alkaline-earth metal oxides, Phys. Rev. B 72 (2005) 125414.

[42] C. D. Valentin, G. Pacchioni, M. Bernasconi, Ab initio molecular dynamics simulation of no reactivity on the cao(001) surface, The Journal of Physical Chemistry B 110 (2006) 8357–8362, pMID: 16623520.

[43] M. S. T. Bukowinski, First principles equations of state of mgo and cao, Geophysical Research Letters 12 (1985) 536–539.

[44] J. F. Mammone, H. K. Mao, P. M. Bell, Equations of state of cao under static pressure conditions, Geophysical Research Letters 8 (1981) 140–142.